

Impact of Nanofluids on Performance of Solar Photovoltaic-Thermal Panel and Heat Pipe Hybrid System

S. Sami^{#1*2}

¹ Research Center for Renewable Energy, Catholic University of Cuenca, Cuenca, Ecuador

² Trans Pacific Energy, Inc, NV, USA, 89183

Received Date: 09 March 2021

Revised Date: 17 April 2021

Accepted Date: 19 April 2021

Abstract — Numerical modeling and prediction of the impact of nanofluids as heat transfer fluids in a hybrid system composed of photovoltaic-thermal solar panels and heat pipe are presented hereby. The model was developed to describe the steady-state and dynamic thermal behavior of the hybrid system composed of a photovoltaic-thermal solar panel with heat pipes under different conditions: solar irradiances, material properties, ambient, and nanofluid flow conditions, different refrigerants contained in the heat pipes under boundary conditions. The model was presented to assess the performance and energy conversion process of the hybrid system as well as the individual efficiencies to produce hot water and electricity. The nanofluids used as heat transport fluid were; Al_2O_3 , Fe_3O_4 , CuO , and SiO_2 . The study demonstrated that nanofluid CuO has higher performance at higher evaporator entering temperatures, and the use of nanofluid CuO resulted in higher heat transfer through the heat pipe compared to the other nanofluids under investigation. The results also showed that the higher the concentration of the CuO , the higher the thermal energy. The results also showed that the higher the concentration of the CuO , the higher the thermal energy delivered to the evaporator section of the heat pipe and consequently increased the hybrid system efficiency of the system in question. This has been observed for all solar radiations and concentrations of nanofluids in this paper. Finally, the presented model has been validated, and its prediction is fairly compared with available data.

Keywords — Numerical modeling, simulation, photovoltaic-thermal solar, heat pipe, refrigerants, nanofluids, hybrid system performance, model validation.

I. INTRODUCTION

A heat pipe is a heat exchanger that transfers heat using the phase change and capillary action of working fluids and or refrigerants. Heat pipes and gravity-assisted thermosyphons are effective, passive devices that enable high rates of heat transfer using internal phase change mechanisms. It can transfer thermal energy without any pumping power required compared to most heat exchangers. Heat pipes are becoming increasingly popular

as passive heat transfer technologies due to their high efficiency when the appropriate refrigerants are used. Heat pipes are currently used in widespread industrial applications, such as solar, nanoparticles, Rankine cycles, nuclear, thermoelectric modules, and ceramics, in which heat pipe technologies offer many key advantages over conventional practices.

Heat pipes are effective and passive heat transfer devices that are capable of transferring heat through small temperature differences between the heat source and the heat sink [1-29]. A heat pipe is normally made of a sealed copper pipe, vacuumed and filled with working fluid such as refrigerant that boils at low temperatures. [15, 22-26]. The distinct sections of the heat pipes are the evaporator section, the condenser section, and the adiabatic section, where no heat transfer between the refrigerant and heat source or heat sink occurs. Heat absorbed at the evaporator section of the pipe boils the working fluid inside the heat pipe and vaporizes with the latent heat of vaporization. This vapor of the working fluid inside the heat pipe is condensed in the condenser section, where it releases its latent heat of condensation. The condensate working fluid is then channeled back to the evaporator section due to gravity and internal wicks. Readers interested in the comprehensive discussions of the heat pipes' heat transfer mechanisms are advised to consult references [2-3, 15, 20, 24-26].

New PV technologies reported in the literature have been shown to improve the energy utilization efficiency of solar PV. A novel concept of combined photovoltaic-thermal solar panel hybrid system concept has been developed and implemented to improve the solar PV's efficiency [17-20] and [26-29], where the PV cells of the solar PV panels are cooled by water flow to absorb the excess thermal energy dissipated due to the intrinsic conversion efficiency limitation of the cell. This, in turn, enhances the conversion efficiency of the cell. Therefore, the net result is an enhancement of the combined photovoltaic-thermal efficiency of the hybrid system. The excess thermal energy absorbed by the cold-water flow through the heat exchanger thermal panel soldered underneath the PV's cell can be used for various domestic



or industrial applications.

The performance of conventional thermal systems that use heat transfer fluid (HTF) has been reported by Poplaski et al. [8] to be improved by adding nanoparticles within the HTF (nanofluid); of Al₂O₃, CuO, and TiO₂ nanoparticles. This work reviewed past studies focusing on the application of nanofluids in various types of heat pipes. Furthermore, full numerical simulation was also presented to account for the effect of nanofluids in a conventional heat pipe. Validation of the numerical model was performed through comparison to experimental tests for various nanoparticles. The optimal nanoparticle concentration of Al₂O₃, TiO₂, and CuO corresponding to the capillary limit for a conventional nanofluid-filled heat pipe was determined to be 25% by vol. for both Al₂O₃ and TiO₂, and 35% for CuO. Overall, a maximum decrease in total thermal resistance was observed to be 83%, 79%, and 76% for Al₂O₃, CuO, and TiO₂, respectively.

Nanofluid behavior and enhancement have also been investigated for various convective and phase-change applications by You et al. [18], who experimentally studied the thermal behavior of aqueous Al₂O₃ nanofluids for pool boiling at different nanoparticle concentrations. His experiment indicated a ~200% increase in the critical heat flux compared to that for the pure water case. However, he reported that the nucleate boiling heat transfer coefficients appeared to be equal for both cases.

Shafahi et al. [22] used a two-dimensional steady, compressible analytical approach employing effective fluid properties to obtain the velocity, pressure, temperature, and maximum heat transfer limit for a conventional screen-wick cylindrical heat pipe charged with aqueous Al₂O₃, CuO, and TiO₂ nanoparticles. The effect of particle diameter and nanoparticle concentration was studied under the assumption of a constant condenser wall temperature. The study showed that the overall heat transfer of the heat pipe increased with the concentration of nanoparticles, and the optimum concentration of each nanoparticle in the base fluid was identified.

Do and Jang [19] studied nanofluid enhancement in heat pipes and formulated two different analytical models under the assumptions of one-dimensional steady axial incompressible flow, a one-dimensional axial temperature difference in the heat pipe wall, and negligible convection in the liquid and vapor phases to the heat transfer and thermal resistance of the heat pipe concerning an enhanced effective thermal conductivity of the working fluid. Also, the authors simulated heat transfer in the heat pipe due to the increased surface area of the highly conductive deposition layer of nanoparticles surrounding the grooved wick structure. Their study concluded that the thermal resistance of the nanofluid charged heat pipe is dependent on two opposing phenomena. They also reported that the thin deposition layer of nanoparticles in the evaporator causes increased liquid pressure to drop within the porous nanoparticle layer. This limited evaporative heat transfer. However, the deposition of nanoparticles resulted in additional conductive surface

area in the evaporator section wick structure that increased heat transfer.

A review on the use of nanofluids in heat pipes has been recently reported by Mohammad Alhuyi Nazari et al. [23], where the thermophysical properties of having studied in various types of heat pipes. To have fluids with higher thermal conductivity, nanoparticles have been added. In reference [23], the effects of using nanofluids in several types of heat pipes were reviewed. The nanofluids in the study were categorized based on the types of particles. The literature review showed nanostructures in the base fluid can significantly reduce the thermal resistance of heat pipes compared with utilizing pure as the operating fluid. It was observed that using graphene oxide/water nanofluid in pulsating heat pipe reduces the thermal resistance up to 42% in comparison with the water-filled heat pipe. Besides, the literature review revealed that the type of nanoparticle, concentration, and stability are among the most important parameters affecting thermal performance. The enhancement in the thermal performance of heat pipes by using nanofluids was mainly attributed to the higher thermal conductivity of the nanofluids and an increase in nucleation sites.

Reference [24] investigated the thermal characteristics of the cylindrical sintered wick heat pipe that are investigated using CuO and Al₂O₃ nanofluids. The effect of inclination angle and heat input on the thermal performance of the heat pipe was also studied. The study observed that a reduction of 0.5 wt.%, 1.0 wt.% and 1.5 wt.% of CuO nanofluids were 2.1 °C, 5.9 °C, and 4.7 °C respectively, whereas, for the same concentrations, Al₂O₃ nanofluids obtained only 0.9 °C, 3.6 °C, and 5.3 °C respectively compared with DI water at horizontal position. It was also observed that the thermal resistance of heat pipe was reduced with increasing heat flux at low heat input, and the reduction is diminished for peak loads. The study concluded that the optimum performance could be attained for both CuO and Al₂O₃ nanofluids at a 45° inclination angle. And the evaporation and condensation HTC for CuO and Al₂O₃ have increased by about 32.99% and 24.59%, respectively, nanofluids at 45°.

This paper presents the impact of the nanofluids used in heat pipes as a part of a novel hybrid system composed of the solar photovoltaic-thermal panel and heat pipes. A schematic diagram of the thermal solar-heat pipes hybrid system using nanofluids under study is shown in Figure.1. This novel concept is intended to enhance the energy conversion efficiency by using nanofluids to recover the excess thermal energy dissipated by the energy conversion process of the solar PV panels. This, consequently, enhances the energy conversion efficiency of the solar photovoltaic and the hybrid system.

The conceptual photovoltaic-thermal panel integrated heat pipes design with nanofluids as heat transfer fluid was modeled and analyzed using a two-dimensional dynamic model based upon the heat transfer and fluid flow energy conversion equations. The model was developed to describe the steady-state and dynamic thermal behavior of the hybrid system composed of a

photovoltaic-thermal solar panel with heat pipes under different conditions: solar irradiances, material properties, ambient, and nanofluid flow conditions, different refrigerants contained in the heat pipes under boundary conditions. The predicted results presented herein include the efficiency of the energy conversion process, PV-Thermal characteristics and heat pipes thermal behavior driven by different nanofluids at different concentrations, refrigerants filled in the heat pipes, and finally, the thermal energy recovered by the PV-thermal panels and delivered for domestic and/or industrial use under different conditions.

II. MATHEMATICAL MODEL

The study presented herein is an extension of the modeling reported by Sami [17], where the hybrid system in question is composed of the PV solar panel and Thermal solar tube collector as well as heat pipe heat exchanger is driven by nanofluids heat transfer fluid and thermal tank as shown in Figure.1. This hybrid system consists of a photovoltaic panel soldered to the backside and thin heat exchanger parallel tubes, whereas the nanofluid cooling fluid circulates. The various flow thin tubes are connected to a heat exchanger where the evaporator section of the heat pipe heat exchanger is placed. The nanofluid flow through the thermal solar collector copper pipes and transport the recovered excess heat away from the solar PV panel and thermal panel and transferred to the evaporator section of the heat pipe, as shown in Figure 1.

The heat pipe condenser section is placed in a thermal tank where it releases its thermal energy and heats the water in the thermal tank, and supply hot water for domestic and/or industrial applications.

A. Solar PV MODEL

The solar photovoltaic panel is constructed of various modules, and each module has consisted of arrays and cells. The dynamic current output can be obtained as reported in; Sami[17] and [31];

$$I_p = I_l - I_o \left[\exp \left(\frac{q(V + I_p R_s)}{AkT_c} \right) - \frac{v + I_p R_s}{R_{sh}} \right] \quad (1)$$

- I_p : Output current of the Pv module
- I_l : Light generated current per module
- I_o : Reverse saturation current per module
- V : Terminal voltage per module
- R_s : Diode series resistance per module
- R_{sh} : Diode shunt resistance per module
- q : Electric charge
- k : The Boltzmann constant
- A : Diode ideality factor for the module

Where;

$$I_o = BT^3 c \left[\exp \left(-\frac{E_{go}}{kT_c} \right) \right] \quad (2)$$

And;

$$I_L = P_1 G [1 - P_2 (G - G_r) + P_3 (T_c - T_r)] \quad (3)$$

Where;

The PV cell temperature, T_c , appeared in equations (1) through (3) is influenced by solar radiation, ambient conditions, and wind speed. It is well known that the cell temperature impacts the PV output current, performance, and time-variation can be determined from references [17-31]. The AC power of the inverter output $P(t)$ is calculated as per equation (4) using the inverter efficiency η_{inv} , output voltage between phases, neutral voltage function V_{in} , and for single-phase current I_o and $\cos\phi$ as follows;

$$P(t) = \sqrt{3} \eta_{inv} V_{fn} I_o \cos\phi \quad (4)$$

B. PV Thermal Model

The following thermal analysis is performed for a single PV cell of the solar PV panel, as shown in Figure.1, and it was assumed that all PV cells behave the same; therefore, this analysis can be applied to the whole PV solar panel.

The heat absorbed by the PV solar cell can be calculated by equation (5) as follows [17, 31]

$$Q_{in} = \alpha_{abs} G S_p \quad (5)$$

Where;

- α_{abs} : Overall absorption coefficient
- G : Total Solar radiation incident on the PV module
- S_p : Total area of the PV module

Meanwhile, the PV cell Temperature can be computed from the following heat balance in the equation (6); [17,31];

$$m C_{p_module} \frac{dT_c}{dt} = Q_{in} - Q_{conv} - Q_{elect} \quad (6)$$

T_c : PV Cell Temperature

m_{Cp_module} : Thermal capacity of the PV module t : time

Q_{in} : Energy received due to solar irradiation, equation (4)

Q_{conv} : Energy loss due to convection

Q_{elect} : Electrical power generated

The thermal energy transferred in terms of the heat transfer mechanisms; conduction, convection, and radiation; from the PV cell to the Heat Transfer Fluid (HTF) was determined by the following equations [17, 31];

The heat transfer by conduction;

$$Q_{conduction} = \frac{K_{pv} * \Delta T (T_c - T_m)}{L_{cell}} \quad (7)$$

T_m : Module Back-surface temperature
 K_{pv} : Thermal conductivity of PV cell
 L_{cell} : Length of a PV cell

The heat transfer by convection;

$$Q_{convection} = h_{water} * \Delta T (T_m - T_f) \quad (8)$$

$Q_{convection}$: Energy due to convection
 h_{water} : Heat transfer coefficient
 T_f : Fluid temperature

And the heat transfer by radiation;

$$Q_{radiation} = \varepsilon * \sigma (T_m^4 - T_f^4) \quad (9)$$

$Q_{convection}$: Energy due to radiation
 ε : Emissivity PV cell
 σ : Stefan-Boltzmann constant

The finite-difference formulation of the above equations (1) through (9) was used to determine the heat transfer fluid temperatures at each element where each heat transfer fluid tube is divided into different thermal elements,

$$T_f = T_{f_{in}} + \frac{\delta Q}{m_{water} c_p} * t \quad (10)$$

\dot{m}_{water} : Water mass flow (HTF)
 c_p : Specific heat of the water.
 t : time

δQ : the heat transfer per element

$T_{f_{in}}$: Fluid temperature at the inlet

The thermal energy transferred from the back of the PV cells to the heat transfer fluid (HTF) was obtained by;

$$Q_{thermal} = \dot{m} * C_{p_{water}} * \Delta T (T_{f_{Hx+1}} - T_{f_{in}}) \quad (11)$$

Where;

$Q_{Thermal}$: Energy from the thermal process

$T_{f_{Hx+1}}$: Fluid temperature at thermal element (f+1)

$T_{f_{in}}$: Fluid temperature at thermal element (1)

The total energy transferred to heat transfer fluid was calculated from the integration of equations (6) through (11) written for each element, dx, along the length of each tube.

It is worthwhile mentioning that the important characteristics of the solar panel such as the PV cell and panel temperature are influenced by different factors and, in particular, the ambient conditions such as temperature, humidity, wind speed, among other parameters [31].

The back-temperature T_m of the PV cell and PV panel can be calculated from the heat balance across the PV cell as follows [7,17,31];

$$Q_{in} = m C_{p_{module}} \Delta T = m C_{p_{module}} (T_c - T_m) \quad (12)$$

Where; T_m is the module back-surface temperature.

It was assumed that the T_m is equal to the surface temperature of the heat exchanger tubes welded to the solar PV cell/panel in close contact with the back surface of each of the PV cells. The heat transferred from the back of the PV cell to the heat transfer fluid (HTF) flowing in the heat exchanger tubes as shown in Figure,1 was computed by the following forced heat transfer convection relationship [17,31];

$$Q_{in} = \pi D L H_{water} \Delta T = \pi D L h_{water} (T_m - T_f) \quad (13)$$

Where;

D: Pipe diameter

L: Pipe length

h_{water} : Forced convection heat transfer coefficient

T_f : Fluid temperature

The heat transfer coefficient, h_{water} , can be approximated as [17,31,7];

$$h = \frac{K_w}{D_H} b_2 Re^n \quad (14)$$

Where Re ; is the Reynolds Number and K_w represents thermal conductivity of water, b_2 and n are numerical constants.

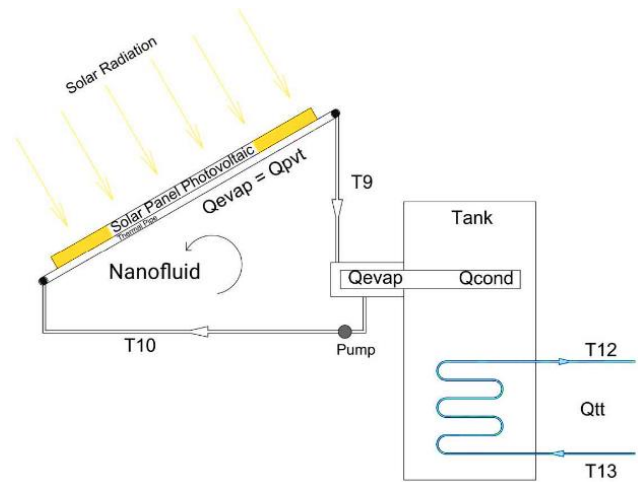


Figure 1: Nanofluids PV-Thermal-Heat Pipe hybrid system

Furthermore, to calculate the heat transfer fluid flow rate circulating in the heat exchanger tubes, the following equation is used with equations (14) and (15);

$$Q_{in} = m_w C_{p_{water}} (T_{f+1} - T_f) \quad (15)$$

\dot{m}_w : represents the Water flow rate

T_{f+1} : Water temperature at the next element.

c_p : Specific heat of HTF.

The total thermal heat transferred to the HTF is obtained after equations (12) through (16)

$$Q_{th} = (\dot{m}_{dot} * n_{pipe}) * (T_{sco} - T_{sco}) * C_{p_w} * \eta \quad (16)$$

Where, m_{dot} : Mass flow rate per pipe the heat exchanger tubes welded to the solar PV cell/panel in close contact to the back surface of each of the PV cells.

n_{pipe} : is the number of tubes of the heat exchanger welded to the solar PV panel.

T_{sco}, T_{sco} : represent the outlet temperature of the solar collector and the inlet temperature to the solar collector, respectively.

η : Heat exchanger efficiency.

The thermal heat transferred to the HTF in equation (17) is fed to the evaporator section of the heat pipe, as shown in Figure.1, where it is absorbed by the refrigerant filled in the heat pipe in the evaporator section and transmitted by the natural circulation of the refrigerant to the condenser section of the heat pipe placed in the thermal tank.

C. Nanofluid Heat Transfer Fluid

The thermophysical, thermodynamic, and heat transfer properties of the HTF with embedded nanoparticles can be determined as a function of the volumetric concentration of the nanoparticles flowing in the fluid flow as in the following equations;

$$\alpha_{total} = \alpha_{particles} + \alpha_{base\ fluid} \quad (17)$$

Where α represents a particular thermophysical property of the nanofluid.

On the other hand, the nanofluid thermophysical properties can be evaluated in terms of the base fluid heat transfer as follows;

$$\alpha_{total} = \alpha_{base\ fluid} + \alpha_{particles}(\phi) \quad (18)$$

Where Φ represents the nanoparticle's volumetric concentration.

Equation (17) relates the specific heat of the nanofluids in terms of the thermal conductivity, thermal diffusivity, and density of the nanofluids as follows; [17, 22, 26, and 31].

$$\lambda = \alpha \rho C_p \quad (19)$$

Where C_p is the specific heat, α is the thermal diffusivity, λ and ρ represent the thermal conductivity and density, respectively.

Interested readers in further details of the calculation of thermodynamic and thermophysical properties such as specific heat, density thermal diffusivity, and thermal conductivity of nanofluids are advised to consult references [17, 22, 26, 30, and 31].

D. Heat Pipe Model

To design of heat pipe and attain the required maximum thermal capacity, the characteristic of the working fluid, the wick, and the container must be determined and considered. For the heat pipe to work properly, the pressure drop in the fluid flow embedded in the heat pipe has to be compensated by the pumping pressure in the wick and the capillarity as prescribed by Sami

[16], Tardy and Sami [20], Endalew [13], and Reay and Kew [28];

$$\Delta P_p = \Delta P_i + \Delta P_v + \Delta P_g \quad (20)$$

Where ΔP_p , ΔP_i , ΔP_v , and ΔP_g are the total pumping pressure, pressure drop for liquid return from the condenser, pressure drop for vapor flow in the evaporator, and gravity head, respectively.

The heat transfer limit for a heat pipe depends on the construction of the heat pipe and the operating environment. The design of the heat pipe and the wick properties are determined by the thermophysical properties of the working fluid used. The heat pipe heat transfer capillary, sonic, entrainment, boiling, frozen start-up, continuum vapor, vapor pressure, and condenser effects determine the physical phenomena that establish the lowest limit of these phenomena and are considered as a design limit. The main design limitations were extensively discussed in Tardy and Sami (29), and Reay and Kew (28), and Tardy and Sami (20), and Sami (16). Interested readers in the capillary, sonic, entrainment limit, and boiling limits of the heat pipes are advised to consult the aforementioned references and others reported in the literature.

Several factors are considered in selecting the working fluid inside the heat pipe; in particular, the working fluid temperature range is an important criterion to be fulfilled. Refrigerants and refrigerant mixtures are widely used as working fluid for low-temperature heat pipes applications because of lower vapor pressure and boiling points.

The energy conversion and efficiency of heat transfer from the evaporator section of the heat pipe to the condenser section in the solar application becomes one of the important selection criteria for the working fluid. Hence, the use of working fluid with higher latent heat is very beneficial to the applications of the heat pipes in solar energy conversion. Water and different refrigerants such as R-134a, R-123, R-32, R-125, R-152a, R-1234ze, and R-1234fz, as well as refrigerant mixtures Sami [38], are considered in this investigation as working fluids inside heat pipe.

Heat pipe using two-phase thermosyphon principles has been reported in the literature and studied by Endalew [13] in water heating applications. On the other hand, References [1-3] are discussed. In the current study, the two-phase in forced convective condensers under either crossflow or parallel flow pattern. In this study, the thermosyphon condition is under consideration, as illustrated in Figure .1. The condenser section of the heat pipe is placed in a thermal storage tank where natural convective heat transfer takes place. It was assumed that

the condensing water flow in the thermal tank is stagnant, and no temperature gradient along the axis of the heat pipe.

The energy balance under natural convection heat transfer condition in the thermal storage tank as per Figure .1, using a single-control volume of heat pipe submerged in the thermal tank is presented in equation (19), [13, 16];

$$V_w P_w C_w \frac{dT_w}{dt} = \pi d_o I_{cond} h_{eff} (T_{hp} - T_w) - U_{tan} A_{tan} (T_{hp} - T_a) \quad (21)$$

Where V_w represents the water volume in the thermal tank and U_{tan} and A_{tan} are the overall heat transfer coefficient in the thermal tank and the equivalent heat transfer area in the tank, respectively. Besides, T_{hp} , T_w , T_a are the temperatures of the heat pipe, water, and ambient air.

On the other hand, the effective heat transfer coefficient h_{eff} of the condenser section of the heat pipe can be given by the following [13, 16]

$$h_{eff} = \left(\frac{1}{h_{cond}} + \frac{1}{h_f} + \frac{\delta_{hp}}{k_{hp}} \right) \quad (22)$$

Where h_f is the natural heat transfer coefficient between the water and the condenser in the thermal tank, δ_{hp} represents the thickness of the heat pipe material, and k_{hp} is the thermal conductivity of the working fluid in the heat pipe.

Also, h_{cond} represents the film condensation heat transfer coefficient and can be obtained from the following correlation suggested by references [13] and [25-28] and using the Nusselt equation;

$$h_{cond} = 0.729 \left(\frac{K_l^3 \lambda \rho_l (\rho_l - \rho_r) g \sin \beta}{\mu_l d_i (T_{hp} - T_w)} \right)^{\frac{1}{4}} \quad (23)$$

Where, T_{hp} , T_w represent the temperatures of the heat pipe and the water in the tank, respectively, and ρ_l , ρ_r are the liquid and vapor densities of the working fluid inside the heat pipe, respectively. And, μ_l , d_i is the viscosity and internal diameter of the heat pipe, respectively.

The natural heat transfer coefficient, h_f between the water in the thermal tank and the condenser section of the heat pipe, and can be developed using the Nusselt equation; [13,16,28] as follows;

$$\frac{h_f d_o}{k_l} = 1.09 \left(\frac{d_o^3 \rho_l^2 g \gamma (T_{hp} - T_w) C_p}{\mu_l k_l} \right)^{\frac{1}{5}} \quad (24)$$

Where; d_o represent the outside diameter of the condenser section of the heat pipe, and C_p is the specific heat of the working fluid inside the heat pipe. And γ is the specific heat ratio. μ_l represents the liquid viscosity of the working fluid.

To determine the heat capacity of the condenser section of the heat pipes, the following energy and mass balance equations are considered;

$$Q_{cond_{hp}} = H_{eff} * (T_{hp} - T_w) * d_o * I_o * \pi \quad (25)$$

Where I_o is the length of the condenser section of the heat pipe.

The efficiency η of the heat exchanger where the heat

pipes are placed can be calculated as;

$$Q_{evap_{hp}} = Q_{th} * \eta \quad (26)$$

On the other hand, the thermal energy dissipated into the thermal tank from the heat pipes and delivered for the domestic or industrial end-user is;

$$Q_{tt} = \eta_{hx} * m_{w_{Qtt}} * C_{p_w} * (T_{12} - T_{13}) \quad (27)$$

Where the $m_{w_{Qtt}}$ Represents the water mass flow rate circulating between the thermal tank and the user application in question. T_{12} and T_{13} are the supply and return temperatures from the end-user application, respectively. η_{hx} is the thermal tank efficiency.

The water mass flow rate for supplying thermal energy to the end-users application is;

$$m_{w_{Qtt}} = \frac{Q_{tt}}{\eta_{hx} * C_{p_w} * (T_{12} - T_{13})} \quad (28)$$

The efficiency of the solar PV panels can be expressed as follows;

$$\eta_{pv} = \frac{Q_{elec}}{Q_{collector}} \quad (29)$$

Where Q_{elec} is calculated by equation (4) and $Q_{collector}$ is obtained by equation (5).

The thermal efficiency of thermal energy transferred to the evaporator section of the heat pipe is;

$$\eta_{Q_{th}} = \frac{Q_{th}}{Q_{collector}} \quad (30)$$

Where Q_{th} is calculated by equation (17).

The thermal efficiency of the heat pipe can be obtained by the following equation;

$$\eta_{hp} = \frac{Q_{cond_{hp}}}{Q_{cond_{hp}}} \quad (31)$$

Where, $Q_{cond_{hp}}$ represents the heat released by the condenser section of the heat pipe and $Q_{cond_{hp}} = Q_{th} * \eta$ where Q_{th} is calculated by equation (16) and η is the thermal efficiency of the heat exchanger where the evaporator section of the heat pipes is placed.

Finally, the hybrid system energy conversion efficiency for harnessing energy from solar energy using the thermal panels and heat pipe can be formulated as;

$$\eta_{sh} = \frac{Q_{evap_{hp}} + Q_{elec}}{Q_{collector}} \quad (32)$$

Where Q_{elec} is calculated by equation (4)

$$\eta_{integ} = \frac{Q_{cond_{hp}} + Q_{elec}}{Q_{collector}} \quad (33)$$

$Q_{cond_{hp}}$ Represents the thermal energy released at the condenser side.

III. NUMERICAL PROCEDURE

Equations (1) through (33) describe the energy conversion and heat transfer mechanisms taking place in the hybrid system shown in Figure.1. The model presented in these equations has been based on mass and energy balances of the individual components of the PV/T hybrid system and the heat transfer fluid circulating in the heat

exchanger thermal thin tubes welded in the back of the PV panel and driving the heat pipe. This permits the calculation of the electrical power output of the solar PV panel, thermal energy recovered from the solar PV panel, and supplied to the heat pipe, using the thermodynamic and thermophysical properties of the nanofluids heat transport fluid and refrigerants in the heat pipe. Finally, the hybrid system's total characteristics and individual efficiencies were predicted at different solar radiation, geometrical parameters, and various boundary conditions.

These energy and mass equations presented in equations (1) through (33) have been solved as per the logical flow diagram presented in Figure 2, where the input parameters of the solar PV- thermal and conditions such as solar radiation, ambient temperature, and humidity as well as other independent and geometrical parameters for the solar thermal tubes geometries and heat pipe characteristics were defined. The dependent parameters were calculated and integrated into the finite-difference formulations. Iterations were performed until a converged solution was reached with an acceptable iteration error.

The numerical solution procedure started with the definition of the solar radiation, ambient conditions to calculate the solar PV cell temperature, and PV cell back temperature, as well as heat transfer fluid mass flow characteristics circulating in the thermal nanofluid closed loop at specified conditions. The thermodynamic and thermophysical properties of nanofluid Heat Transfer Fluid (HTF) were employed to calculate the mass flow rate. This followed by solving the finite-difference formulations to predict the time variation of the different system characteristics such as; PV cell temperature, the PV back temperature, and thermal heat transferred to the Heat Transfer Fluid, Heat transfer fluid outlet temperature at the thin tubes heat exchanger, as well as the water temperature in the thermal storage tank and the nanofluid heat transfer fluid that drives the evaporator section of the heat pipe. This step was followed by the selection of the heat pipe working fluids, refrigerant and refrigerant mixture, operating conditions based upon the thermodynamic and thermophysical properties of the refrigerant circulating in the heat pipe. Finally, other hybrid system characteristics such as the thermal and power outputs and individual efficiencies were calculated as well as the hybrid system efficiency at each input condition.

The thermophysical and thermodynamic properties of the refrigerants considered in this study used in the aforementioned model and needed to close the system of equations were determined using REFPROP software as per references [31,36]. The NIST REFPROP database [36] provides the most accurate thermophysical property models for a variety of industrially important working fluids and fluid mixtures, including the accepted standards ones. It has proven to be an extremely useful and accurate tool in calculating the thermophysical and thermodynamic properties of the refrigerants, such as pressure, temperature, enthalpy.

IV. RESULTS AND DISCUSSION

To solve the aforementioned conservation equations (1) through (33) and taking into account the heat and mass transfer mechanisms during the solar PV thermal and heat pipe energy conversion processes, the above-mentioned equations were coded, integrated using the finite-difference formulations, and solved as per logical flow chart depicted in Figure.2. Besides, for validation, the predicted simulated results for PV-Thermal solar panels were compared to the data. In the following sections, we present an analysis and discussion of the numerical results predicted as well as validations of the proposed simulation model. The simulations were performed at fixed temperature differences across the thin heat exchanger flow pipes bonded to the back of the solar PV panel. However, only results will be presented and analyzed for the temperature difference of 15 °C across every single thermal tube. It is worthwhile noting that the numerical simulation presented hereby was conducted under different conditions such as; PV cell temperatures from 10°C through 70°C, ambient temperatures from 10°C through 38°C and solar radiations; 550, 750, 1000, and 1200 w/m² as well as different nanofluids; Ai₂O₃, Cuo, Fe₃O₄, SiO₂ at different concentrations; 5% to 20% and refrigerants filled in the heat pipe with lower Global Warming Potential (GWP) such as R134a (HFC 134a), R123 (HCFC 123), R125 (HFC 125), R32 (HFC 32), R152a (HFC 152a), R1234ze (HFO 1234ze), R1234fz(HFO 1234zf). Thermodynamic and thermophysical properties were obtained using the methodology outlined and presented in references [16, 31].

The recording of the ambient conditions during this work showed that the relative humidity is stable during the various hours of the day. It is quite apparent from recorded data that the peak solar irradiation and maximum temperatures occur at midday. Average solar irradiation and ambient temperatures were used in the modeling and simulation of the Photovoltaic panels, and the simulation of the PV thermal solar panel relative humidities was assumed constant.

The PV characteristic curves are given in the manufacturer's specification sheet. The PV panel characteristic curves under consideration in this study are obtained from Sami and Campoverde [31]. Among the parameters used in this study are; Total surface area of the PV module (SP) is 0.617 m², Total surface area of cells in module (Sc) is 0.5625 m², module efficiency 12% at reference temperature (298 K), the overall absorption coefficient is 0.73, and Temperature coefficient is 0.0045 K⁻¹. Interested readers in the full range values of the other parameters are advised to consult Faragali et al. [31].

The PV characteristic curves are given in the manufacturer's specification sheet. The PV panel characteristic curves under consideration in this study are obtained from references [16, 31]. Among the parameters used in this study are; Total surface area of the PV module (SP) is 0.617 m², Total surface area of cells in module (Sc) is 0.5625 m², module efficiency 12% at reference temperature (298 K), the overall absorption coefficient is

0.73, and Temperature coefficient is 0.0045 K-1. Interested readers in the full range values of the other parameters are advised to consult reference [16, 31].

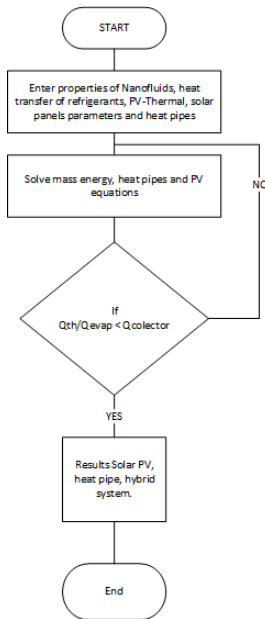


Figure.2 Logical flow diagram for solving PV-Th and Heat Pipes

It was also assumed in this simulation that the whole solar panel was covered in PV cells with no packing material. A material used to fill in gaps between the cells on a panel. The PV cells are commercial grade monocrystalline silicon cells with an electrical efficiency of 12% and have a thermal coefficient of 0.54% [1/K]. However, it depends upon the rated solar radiation [16, 31]. The thermal coefficient represents the degradation of PV cell output per degree of temperature increase. The thin heat exchanger pipes were strongly bonded to the back of the PV solar model without any air gap to ensure complete heat transfer by conduction, convection, and radiation to the heat transfer fluid flowing in the thermal pipes. The exiting temperatures of heat transfer fluid vary between 25 C° to 75 C°. This heat transfer fluid drives the evaporator section of the heat pipe, and the thermal heat absorbed from the heat transfer fluid evaporates the refrigerant in the evaporator section of the heat pipe. The vapor of the refrigerant was then circulated by natural convection and carried to the condenser section of the heat pipe, where it was condensed and released its heat of condensation to the water in the thermal storage tank.

As can be seen from equations (6) through (15), an increase in the PV cell temperature will result in an increase in the back-cell temperature and consequently the temperature of the heat transfer fluid. Consequently, this increases the thermal heat driving the evaporator section of the heat pipe and increases the thermal energy transferred by the heat pipe condenser section to the thermal storage tank. It has also been reported by references [16, 31] that the higher the cell temperature, the higher the back cell and higher fluid temperatures as well as the thermal energy delivered to the evaporator section

of the heat pipe. Also, the higher the solar radiations, the higher the energy absorbed by the PV cell, and consequently, the higher the temperature of the cell until it reaches the design temperature [16, 31]. However, it was also reported that the changes in the PV cell temperature caused by solar radiation have a dynamic nature, as observed in Figure.3. The PV panel heats up and cools down gradually depending upon the changes in solar radiation in dynamic response and consequently the power output from the PV panel. This has been reported and discussed in the literature, where similar observations were presented in references [16, 31].

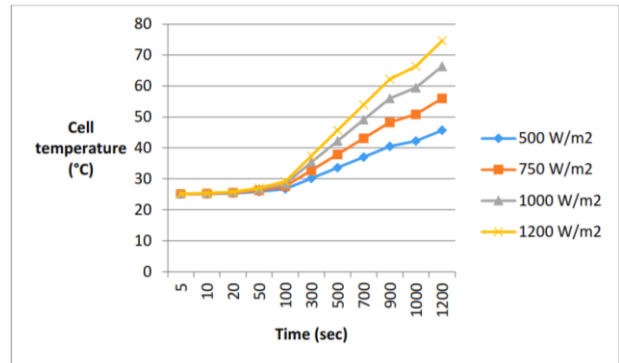


Figure.3 PV cell temperature dynamic characteristics at different solar radiations and temperature difference of 15 °C across thin tubes heat exchanger.

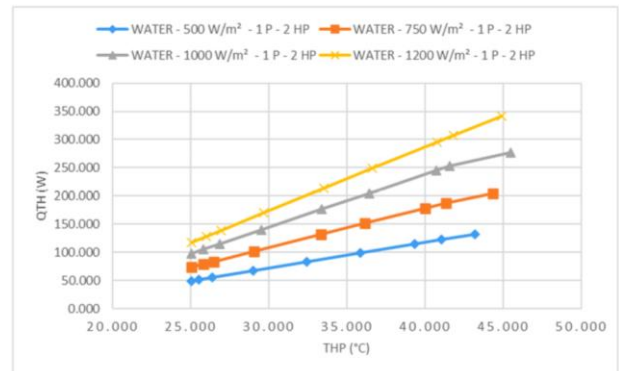


Figure.4 Thermal Heat released at different solar radiations at one solar PV panel at different heat pipe temperatures and two heat pipes filled with water.

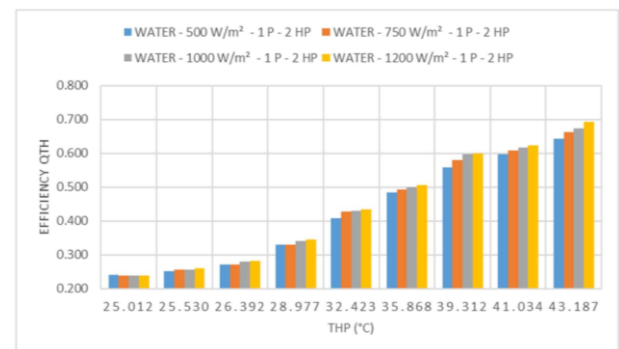


Figure.5 Efficiency of Heat released at different solar radiations and temperatures at one solar PV panel with two heat pipes filled with water.

Figure.4 presents the thermal heat released from one solar PV panel at different solar radiations and heat pipe temperatures for two heat pipes. The working fluid filled in the heat pipe was water. The heat pipe temperature was defined as the temperature where the heat pipe's evaporation and condensation of the working fluid taking place. The heat balance performed suggested that two heat pipes result in the optimized performance of the hybrid system in question. The results presented in this figure using water as working fluid showed that the higher the solar radiations, the higher the thermal energy absorbed by the heat transfer fluid. Besides, at specific solar radiation, the higher the thermal heat transferred to the heat transfer fluid and the evaporator section of the heat pipe, the higher the heat pipe temperature.

The Efficiency of thermal Heat released and calculated by equation (28) at different solar radiations and heat transfer fluid temperatures for one solar PV panel with two heat pipes filled with water has been plotted in Figure.5. As per equation (28), the thermal heat efficiency is defined as the heat transferred divided by the solar radiation absorbed by the PV panel. It is quite evident from the results presented in this figure that the higher the solar radiation, the higher the thermal conversion efficiency.

The thermophysical, thermodynamic, and heat transfer properties of the HTF with embedded nanoparticles can be determined as a function of the volumetric concentration of the nanoparticles flowing in the fluid flow as per equations (15) through (17).

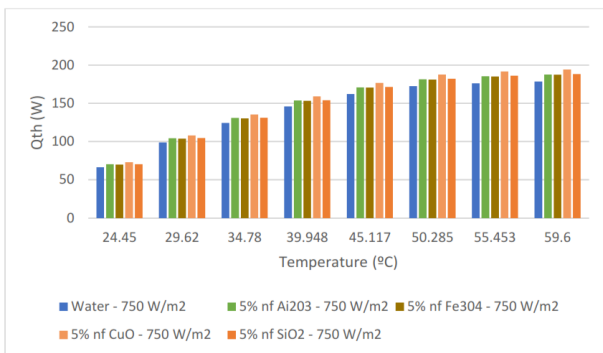


Figure. 6 Thermal energy at HTF temperatures

Equations (19) through (23) were used to determine the thermal heat released by the condenser section of the heat pipe in the storage tank. Figures 6 through 10 have been constructed to analyze the results of the thermal heat released by the condenser section. The performance of the heat pipe using water as well as different refrigerants as a working fluid were plotted at different nanofluids and 750 w/m² solar radiation and heat pipe temperatures. The results presented in these figures showed that nanofluid CuO has a higher thermal heat released by the condenser section of the heat pipe. Furthermore, the higher the heat pipe temperature, the higher performance of the heat pipe and the hybrid system.

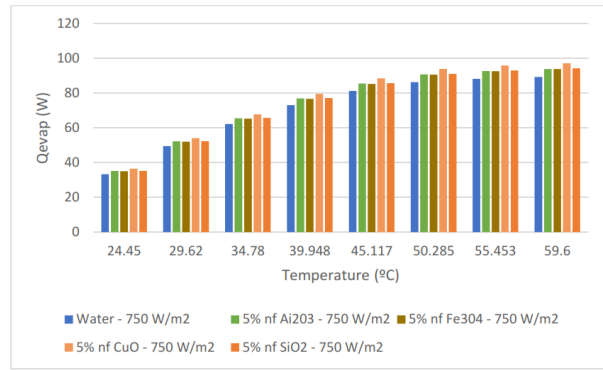


Figure. 7 Thermal energy of evaporator at HTF temperatures

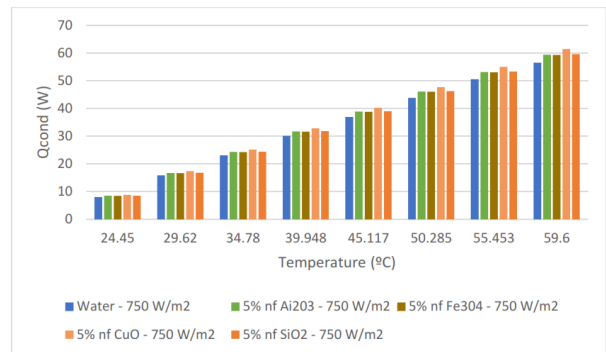


Figure. 8 Thermal energy of condenser at HTF temperatures

The thermal heat transferred to the heat pipe evaporator section and released by the condenser section to the water in the storage tank is plotted and presented in Figures. 8 through Figure 10 at 750 w/m² solar radiations and different nanofluids This was necessary to examine the impact of the different nanofluids on the heat pipe's performance. The results displayed in these figures demonstrated that nanofluid CuO has higher performance at higher evaporator entering temperatures and the higher the thermal heat released to the storage tank from the heat pipe condenser section. Similar behavior has been observed with other refrigerants used in this investigation.

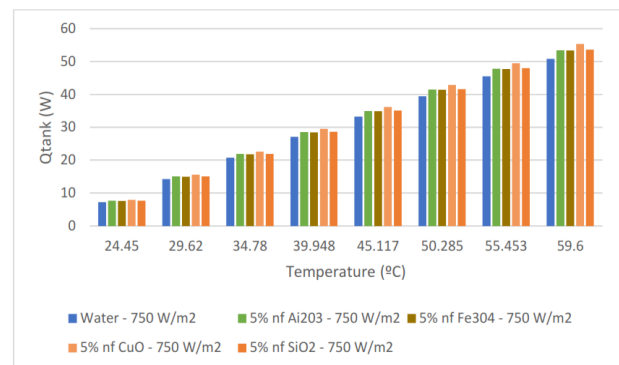


Figure. 9 Thermal energy transferred to the storage tank at HTF temperatures

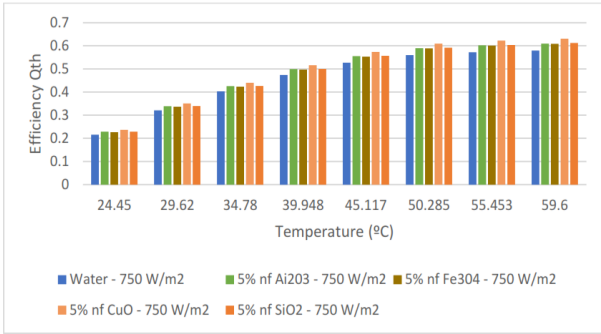


Figure. 10 Efficiency of Thermal energy at HTF temperatures

Figures.8 and 9 quantified the heat released by the condenser section of the heat pipe and dissipated into the storage tank using nanofluids as working fluid. Furthermore, at constant solar radiation, higher heat transfer fluid temperatures resulted in higher heat released by the condenser section. Besides, it is evident from the results presented in the aforementioned figures that the use of nanofluid CuO resulted in higher heat transfer through the heat pipe compared to the other nanofluids under investigation. This has been observed for other solar radiations and concentrations of nanofluids, as discussed later in this paper.

The Efficiency of the heat pipe can be calculated using equation (29). It appears from the results presented in Figure.10a that the higher the heat pipe temperature, the higher the heat pipe efficiency. As mentioned above that higher heat transfer fluid temperature resulted from higher solar radiation and the use of the different nanofluids.

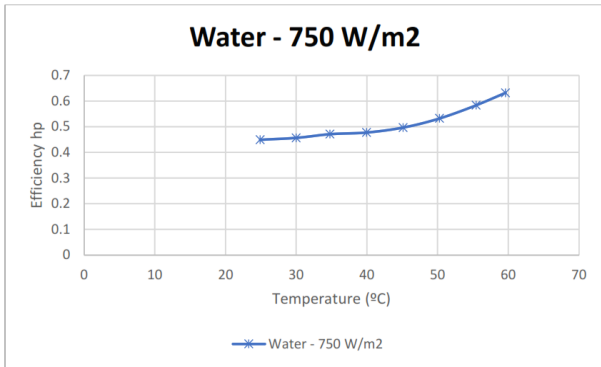


Figure. 10a Efficiency of Heat Pipe at HTF temperatures

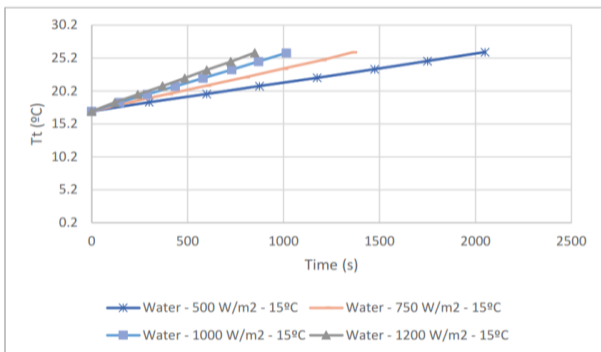


Figure. 11 Storage tank temperature at different time

Endale [13], Sami [19], Tardy and Sami [23], and Reay and Kew [28] reported that the thermal capacity, the characteristic of the working fluid, the wick, and the container of the heat pipe determine the condenser section thermal capacity of the heat pipe as per equations (18) through (23). It has been observed during this study that the limitations imposed by the aforementioned parameters determine the amount of heat released by the condenser section of the heat pipe. As mentioned, higher solar radiation resulted in higher heat pipe temperatures. This could cause higher heat losses during the energy transfer process inside the heat pipe. Therefore, it is believed that higher solar radiation does not necessarily result in higher heat pipe efficiency. It is recommended that the selection and design of the heat pipe are based upon the selection of the appropriate geometry of the heat pipe to maximize the energy conversion efficiency of the heat pipe at particular solar radiation.

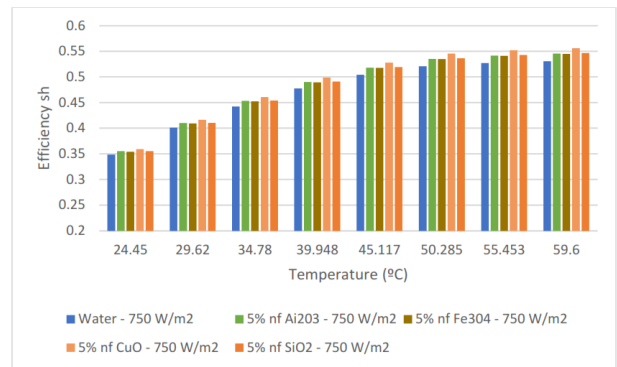


Figure. 12 Efficiency of the Hybrid system at HTF temperatures

On the other hand, the thermal energy released by the condenser section of the heat pipe placed in the thermal storage tank, as shown in Figure.1, increased the temperature of the water gradually, as displayed in Figure.11 under different solar radiations. It can be shown that the solar radiation and the heat pipe temperature, the higher the water temperature in the thermal storage tank.

It can also be noticed from the aforementioned figures that the higher the temperature of the heat pipe, the higher the thermal heat released by the condenser section of the heat pipe. This is one of the most important features of using a heat pipe where the thermal heat absorbed at the evaporator section of the heat pipe is released in the thermal tank with the help of the natural circulation of the working fluid filled in the heat pipe without any input power and the only source of energy required for this energy conversion process is the solar radiation.

The efficiency of the hybrid system and hybrid Integral system were calculated by equations (30) and (31). In particular, the Hybrid Integral system efficiency represented the hybrid system, including the heat pipe, while the hybrid system efficiency excluded the heat pipe. Both efficiencies have been plotted in Figure.12 and Figure.13. at different conditions. In particular, Figure.12 presented and discussed the dependency of the hybrid system efficiency on the thermal energy transmitted to the

heat pipe evaporator section, while Figure .13 depicted the dependency of the hybrid integral efficiency on the condenser section. It can easily be pointed out from the results plotted in these two figures .12 and .13 that the nanofluid CuO has the highest hybrid system and integrated efficiency among the other nanofluids used in this study. It is believed that this observation is due to the higher thermophysical and thermodynamic properties over other nanofluids under investigation. Similar results were observed at other concentrations of the CuO nanofluids.

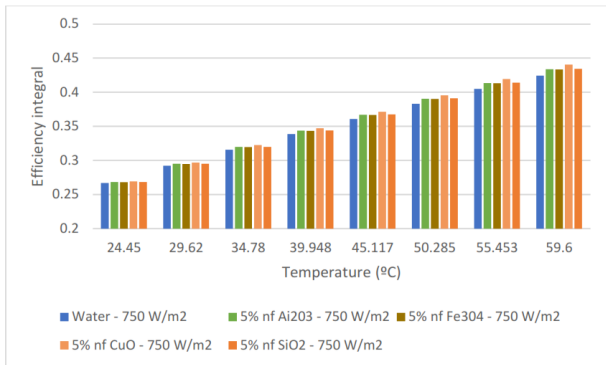


Figure. 13 Efficiency of the Hybrid Integral system at HTF temperatures

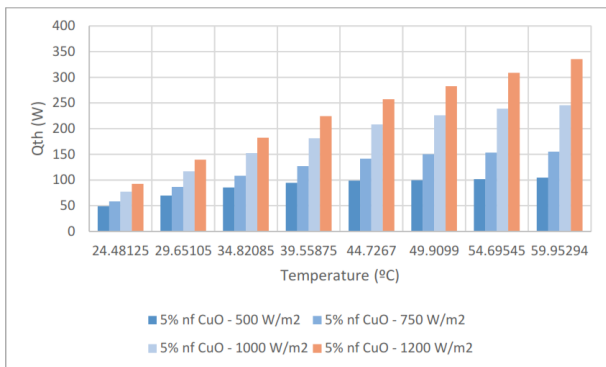


Figure. 14 Thermal energy absorbed at PV-TH with different nanofluids

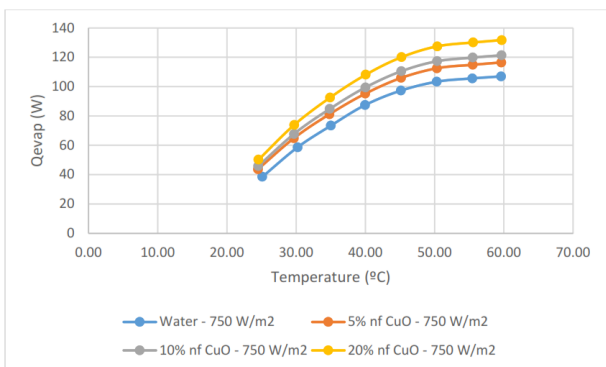


Figure. 15 Thermal energy delivered to the heat pipe evaporator section

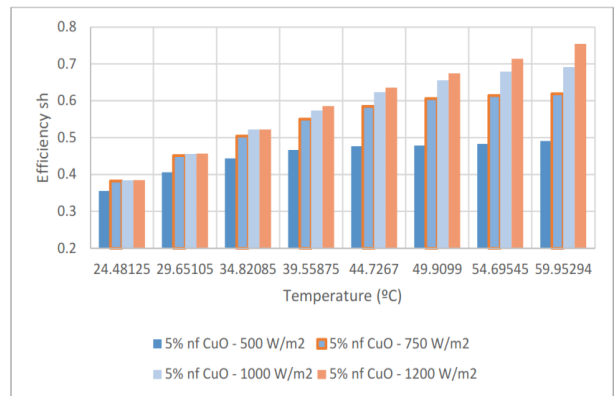


Figure. 16 Efficiency of the Hybrid system at different solar radiations.

The effect of nanofluid concentration on the thermal energy driving the heat pipe evaporator section was demonstrated in Figure. 15. Where a comparison between the nanofluid CuO as heat transfer fluid at different concentrations compared to water as base heat transfer fluid. The results showed that the higher the concentration of the CuO, the higher the thermal energy delivered to the evaporator section of the heat pipe and consequently increased the hybrid system efficiency of the system in question.

To study the impact of solar radiations, Figures 15 and 16 have been constructed at CuO concentration of 5% and the initial temperature of nanofluid CuO at 15°C at different solar radiations. It was evident from the results presented in these figures that the higher the solar radiation, the higher the thermal energy transfer to the nanofluid CuO circulating in the thermal loop as per Figure.1. Also, as shown in these figures, the higher the solar radiation, the higher the nanofluid heat transfer temperature. Similar results were observed at other concentrations of the CUO as well as for other nanofluids, Ai2O3, Fe3O4, and SiO2.

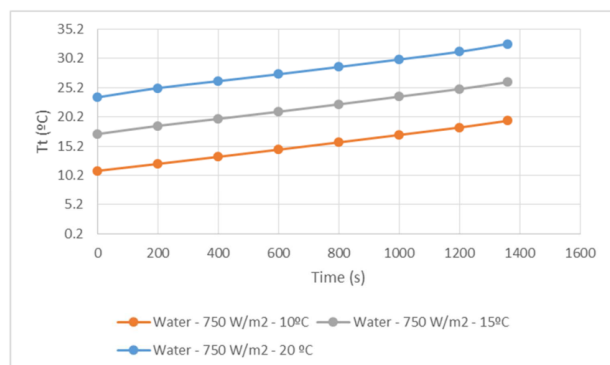


Figure.17 Water temperature in the thermal tank with the condenser section of the heat pipe

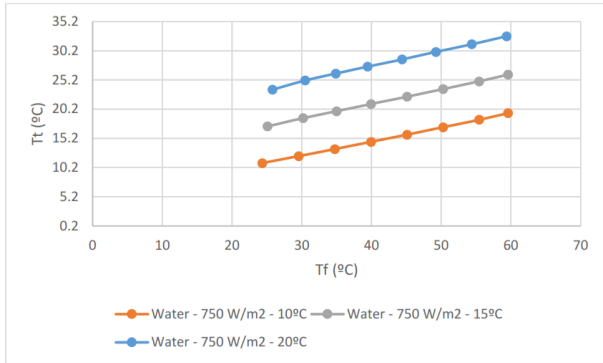


Figure.18 Water temperature in the thermal tank with condenser section of the heat pipe at different HTF temperatures

Furthermore, as shown in Figure.1, this novel concept is intended to enhance the energy conversion efficiency of the PV-Thermal solar hybrid system by utilizing the excess thermal energy dissipated in the nanofluids heat transfer fluid to drive heat pipe to produce hot water stored in the thermal tank.

This process also enhances the energy conversion efficiency of the solar photovoltaic panel's system. As shown in Figures 17 and 18, the thermal energy dissipated from the PV-Th panels increased the water temperature in the thermal tank, and also can be observed that the higher the temperature of the nanofluid heat transport fluid, the higher the water temperature in the tank. Also, as shown in Figure .16, the PV system efficiency has been increased with the use of the heat pipes from the PV solar panel efficiency at 22.38 % alone.

Equation (21) was used to describe the mass and energy balances under natural convection heat transfer in the thermal tank for a single-control volume of heat pipe submerged in the thermal tank [9] and was used to calculate the water temperature. However, it has been reported that the amount of thermal heat transferred into the thermal tank and impacted the water temperature depends upon the type of refrigerant filled in the heat pipe [16, 28, and 29].

Furthermore, examining the results presented in Figures 6 through 18 indicated that the higher the solar radiations, the higher the evaporator temperatures, and obviously the higher the heat released from the heat pipe condenser.

Figure 19. has been constructed to show the impact of the different solar radiations, 500 through 1200 w/m2, on heat transfer in the tank. It is evident from the results displayed in this figure that the higher the solar radiation, the higher the heat transfer to the water in the thermal tank. This is attributed to the fact that the higher the solar radiation, the higher the thermal energy transferred to the evaporator section of the heat pipe and consequently to the condenser section of the heat pipe and the thermal tank. It is quite important to the designer of this system to properly select the site where the solar radiation is the highest to benefit from the higher thermal energy transfer to the water in the thermal tank and the higher thermal efficiency of the system in question.

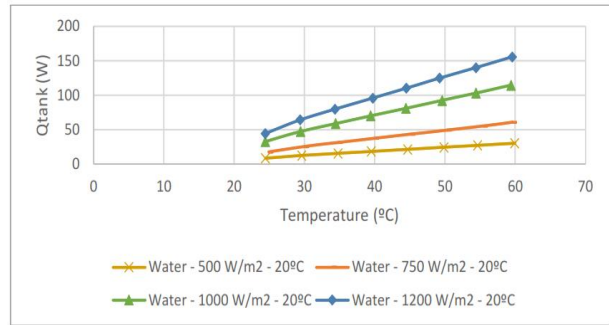


Figure.19 Thermal energy transferred to water in the thermal tank.

The dynamic behavior of the water temperature in the thermal tank is plotted in Figure. 18 against time for different supply water temperatures from the solar collector. It is quite clear from the data presented in this figure that the higher the supply temperature from the solar collector, the higher the water temperature in the thermal tank. Besides, it can be pointed out that the water temperature in the thermal tank for domestic or industrial use can be reached after 5 hours depending upon the solar collector supply temperature. As also shown in Figure.19, and previously discussed, the higher the solar radiation, the higher the supply water temperature of the solar collector, and the thermal energy transferred to the water in the tank, thus, Figures 18 and 19. Demonstrated clearly that the higher the solar radiation, the higher the water temperature in the thermal tank.

Finally, we believe that the designer of the PV-T integrated heat pipe must ensure that the PV solar panel characteristic, cell temperatures, site solar radiation, the ambient conditions, and the refrigerant filled in the heat pipe characteristics and thermodynamic properties are taken into consideration in the decision making and selection of the different components of the PV-Thermal system.

V. MODEL VALIDATION

To validate the numerical model prediction describing the novel hybrid system under investigation and presented in Equations (1) through (33), data available in the literature for the solar PV-Thermal panel were used. In the following sections, we discuss the model validation in predicting the PV-Thermal solar panel and heat pipe characteristics. The basic prediction of the model performance was based upon the determination of the PV solar panel characteristics, cell temperatures, and heat dissipated from the solar PV-Thermal panel and used to drive the heat pipe. To this end, we have constructed Figures 20 to compare the proposed model prediction of the PV solar cell temperatures with the experimental data presented in the literature on the PV cell temperature, namely Sami and Campoverde [31] and Faragali et al. [41].

In particular, as shown in Figure 20, it is quite apparent from the comparison presented in this figure that the model prediction fairly compares with the data of the dynamic PV cell temperature presented by Faragali et al.

data [41]. The comparison presented in this figure also showed some discrepancies existed. It is believed that the discrepancies were because Faragali et al. [41] did not provide full disclosure of the various parameters used in equations (6) through (9). However, as pointed out in references [31 and 33], because of the complexity of the PV cell temperature phenomena and its thermal behavior, we feel that our model fairly predicted the PV cell dynamic profile.

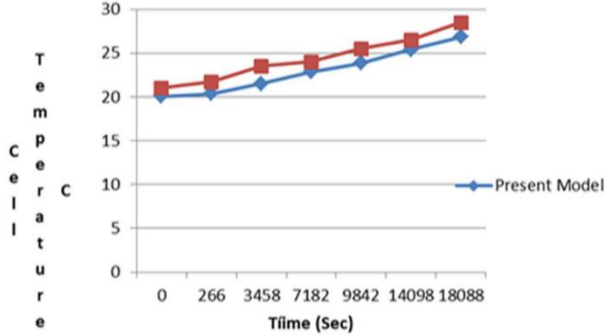


Figure. 20 Model's prediction of the cell temperature with experimental data [31].

Furthermore, Figure. 21 also showed a comparison between the model's prediction and experimental data presented in [31 and 33], where the numerical prediction of the characteristics of the solar PV panel in terms of the power a different amperage that varies with solar radiations were displayed. It is evident from this figure that the present model predicted fairly the solar PV characteristics.

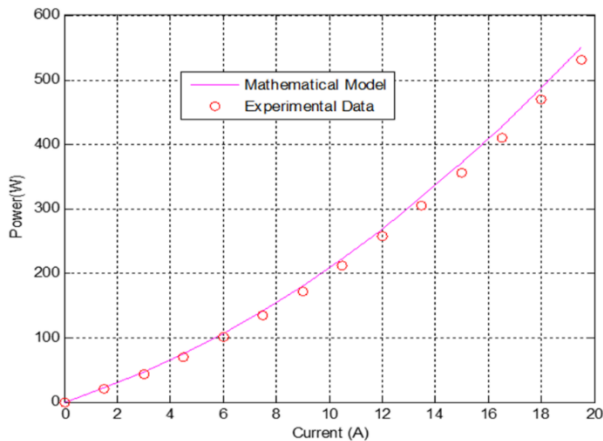


Figure. 21 Comparison between model and experimental data [31 and 33]

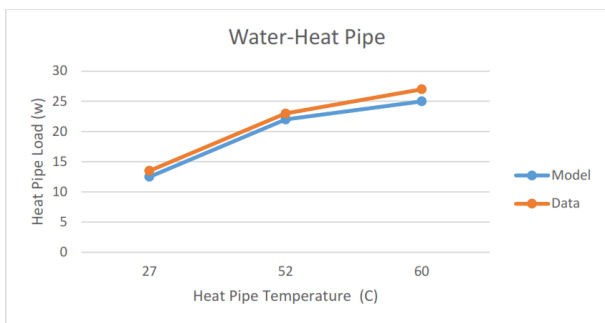


Figure.22 Comparison between model and experimental data [40]

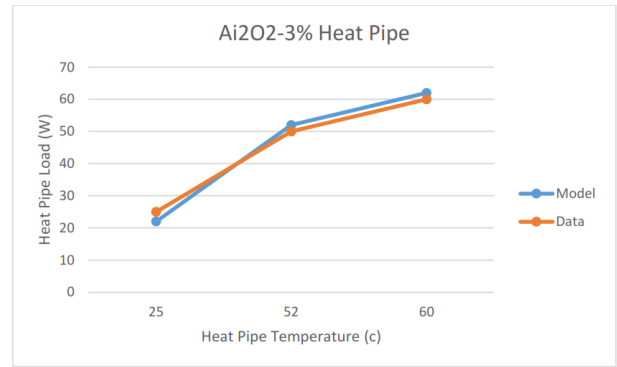


Figure.23 Comparison between model and experimental data [40]

On the heat pipe performance, Figures 22 and 23 have been constructed to compare the numerical model values and experimental data reported in reference [40] for water and nanofluid Ai2O2 as heat transfer fluid. The comparison presented in the two figures showed a fair agreement between the experimental data and the model prediction. However, it appeared that the model slightly over-predicted the data for Ai2O2 nanofluid and under-predicted the data for water. This could be attributed to the lack of the test conditions and the wide range of temperatures where data were collected reported in reference [40].

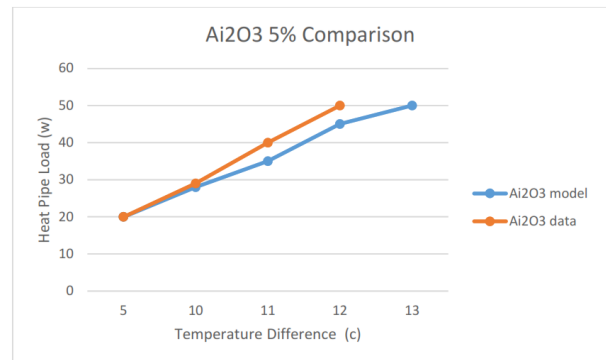


Figure.24 Comparison between model and experimental data [39]

Finally, the comparison has been displayed in Figure.24 between the model's prediction of the heat pipe load and the temperature difference across the heat pipe and the experimental data reported in reference [39]. This reference examined the effect of nanofluids on heat pipes on the subject of temperature parameters and thermal resistance in the heat pipes. The results in Figure 24 demonstrated clearly that our model predicted the heat pipe's heat load of the nanofluid Ai2O3 fairly. This comparison also showed that some discrepancies existed between the model's prediction and the data presented by reference [39], and the data were underpredicted. We are in the opinion that this was attributed to the fact that the calculation of the heat transfer coefficient in the heat pipe model did not fully take into account the heat losses taking place during the energy transfer conversion during this process.

VI. CONCLUSIONS

The energy conversion equations describing the mass and energy balances have been developed, integrated, and solved to predict the characteristics and key parameters of the hybrid system composed of PV-Thermal and heat pipe using different nanofluids. The model is based on dynamic mass and energy equations coupled with the heat transfer coefficients, and thermodynamic constants, and as well as nanomaterial properties. This hybrid system in question is composed of the novel combined concept of a photovoltaic-thermal solar panel PV and heat pipe with nanofluids used as heat transport fluid.

As PV solar panel efficiency calculations showed, the higher the solar radiation, the higher the solar PV current, and consequently, this increases the solar PV power output. However, the PV solar panel efficiency remains constant at 22.38 %.

It is quite clear from the results presented during this investigation that the higher the solar radiations, the higher the evaporator temperatures and heat pipe temperature and obviously the higher the thermal heat transferred to the heat pipe evaporator section and consequently the higher the heat released from the heat pipe condenser section in the thermal tank. Furthermore, the data also shows that the higher solar radiation, the higher the heat pipe temperature, the higher the heat pipe efficiency, and the higher the water temperature in the thermal tank, which is supplied to the domestic or industrial demand.

The results displayed in these figures demonstrated that nanofluid CuO has higher performance at higher evaporator entering temperatures, and the use of nanofluid CuO resulted in higher heat transfer through the heat pipe compared to the other nanofluids under investigation. The results also showed that the higher the concentration of the CuO, the higher the thermal energy delivered to the evaporator section of the heat pipe and consequently increased the hybrid system efficiency of the system in question. This has been observed for all solar radiations and concentrations of nanofluids in this paper.

Finally, the present model predicted well the solar PV characteristics and the thermal behavior of the heat pipes as well as the water temperature dynamic profile.

NOMENCLATURE

$Area_{cell}$	PV cell area (m ²)
$Area_{pipe}$	Pipe area (m ²)
Area	Heat transfer area (m ²)
Cp_{water}	Thermal capacity of water (J/kgK)
D	Internal Pipe diameter (m)
E_{gO}	Bandgap energy of the semiconductor (1.1 eV)
G	Total Solar radiation incident on the Pv module (W/m ²)
H	Convective heat transfer coefficient module (W/m ² K)

h_{water}	Heat transfer coefficient (W/m ² K)
h	Refrigerant enthalpy
I	Output current of the Pv module (A)
I_o	Diode saturation current per module (A)
I_{ph}	Light generated current per module or photocurrent (A)
I_{rs}	Module reverse saturation current (A)
I_{sc}	Short circuit current (A)
K	Boltzmann's constant (1.3806503*10 ⁻²³ J/K)
K_i	Short-circuit of a Pv cell at SRC (mA/°C)
K_{pV}	Thermal conductivity of Pv cell (W/mK)
L_{cell}	Length of a Pv cell (m)
\dot{m}	Water flow (Kg/s)
m_{Cp_module}	Thermal capacity of the Pv module (9250 J/K)
m_{water}	mass of water (Kg)
n	Ideality factor of the diode (q)
N_p	Total number of cells connected in parallel
N_s	Total number of cells connected in series
n_{TE}	number of Thermal Elements in a pipe
P	Power generated by Pv module (W)
Q	Electronic charge (C)
$Q_{conduction}$	Energy due to conduction (W in Electrical Process) (W/m ² in Thermal Process)
$Q_{convection}$	Energy due to convection (W in Electrical Process) (W/m ² in Thermal Process)
Q_{elect}	Electrical power generated (W)
Q_{in}	Energy received due to Solar irradiation (W/m ²)
Q_{in_cell}	Energy incident on one PV cell due to solar radiation (W/m ²)
$Q_{radiation}$	Energy due to radiation (W/m ² in Thermal Process)
$Q_{Thermal}$	Energy from the thermal process (W)
R_d	Fouling factor - or unit thermal resistance of the deposit (m ² K/W)
R_s	Diode series resistance per module (Ω)
R_{sh}	Diode shunt resistance per module (Ω)
S_c	Total surface area of PV cells in a module (m ²)
S_p	Total area of the PV module (m ²)
T	Operating temperature (k)
T	Time (s)
T_a	Ambient temperature (°C)
T_c	Pv Cell Temperature (°C)

T_f	Fluid temperature ($^{\circ}\text{C}$)
T_{f_in}	Fluid temperature at the inlet ($^{\circ}\text{C}$)
T_{fHx}	Maximum temperature at the heat exchanger ($^{\circ}\text{C}$)
T_{fHx+1}	Fluid temperature at thermal element 1 (dx) ($^{\circ}\text{C}$)
T_m	Module Back-surface temperature ($^{\circ}\text{C}$)
T_r	Nominal temperature (298.15 K)
V	Output voltage (V)
V_{oc}	Open circuit voltage (V)
V_t	Diode thermal voltage (V)
α_{abs}	Overall absorption coefficient
η_{Hybrid}	Hybrid system efficiency
η_{Pv}	module efficiency
$\eta_{Thermal}$	Efficiency of thermal process
ρ_w	Density of water vapor (Kg/m ³)
δQ	Convection heat transfer rate
Q	Thermal heat (kj/s)
ϵ	Emissivity PV cell

ACKNOWLEDGMENT

The research work presented in this paper was made possible through the support of the Catholic University of Cuenca. The author also would like to thank Edwin Marin for his great help in performing the different computations and graphical presentations.

REFERENCES

- [1] D.J. Yang, Z.F. Yuan, P.H. Lee, and H.M. Yin., Simulation and experimental validation of heat transfer in a novel hybrid solar panel., *International Journal of Heat and Mass Transfer* 55(2012) 1076-1082.
- [2] Gang, P., Huide, F., Toa, Z., and Jie, J., A Numerical and Experimental Study on a Heat Pipe PV/T System, *Solar Energy*, 85(2011) 911-921.
- [3] Dai, N, Li, S., Zhang, Z., Simulation of Hybrid Photovoltaic Solar Assisted Loop Heat Pipe/Heat Pump System, *Appl. Sci.* 7(2017) 2-15.
- [4] Jubin V Jose, A Ramesh, Ebin Joshy., A Review of Performance of Heat Pipe with Nanofluids, *International Journal of Research and Innovations in Science and Technology*, 1(1)(2014) 74-77
- [5] H.T. Chien., Effect of structural character of gold nanoparticles in nanofluid on heat pipe thermal performance, *Materials Letters*58 (2004) 1461-1465(Online: <http://www.sciencedirect.com/science/article/pii/S0167577X03008036>)
- [6] M.G. Mousa., Effect of nanofluid concentration on the performance of circular heat pipe, *Ains Shams Engineering Journal* 2(2011) 63-69 (Online:<http://www.sciencedirect.com/science/article/pii/S209044791100004>).
- [7] Sakhr M. Sultan M.N.Ervina Efzan Review on recent Photovoltaic/Thermal (PV/T) technology advances and applications, *Solar Energy*, 173(2018) 939-954, <https://doi.org/10.1016/j.solener.2018.08.032>.
- [8] Leonard M, Poplaski Steven, P. Benn, Amir Faghri., Thermal performance of heat pipes using nanofluids, *International Journal of Heat and Mass Transfer*,107(2017) 358-371.
- [9] Mashaei, P.R. & Shahyari, M., Effect of Nanofluid on Thermal Performance of Heat Pipe with Two Evaporators; Application to Satellite Equipment Cooling., *Acta Astronautica*, 111(2015) 345–355. <http://www.sciencedirect.com/science/article/pii/S0094576515000430>.
- [10] Buschmann, M.H. & Franzke, U., Improvement of Thermosyphon Performance by Employing Nanofluid., *International Journal of Refrigeration*, 40(2014) 416–428. <http://linkinghub.elsevier.com/retrieve/pii/S0140700713003630>.
- [11] Wan, Z., Deng, J., Li, B., Xu, Y., Wang, X. & Tang, Y., Thermal Performance of a Miniature Loop Heat Pipe Using Water-Copper Nanofluid. *Applied Thermal Engineering*, 78(2015) 712–719. <http://linkinghub.elsevier.com/retrieve/pii/S1359431114009983>.
- [12] Venkatachalapathy, S., Kumaresan, G. & Suresh, S., Performance Analysis of Cylindrical Heat Pipe Using Nanofluids – An Experimental Study. *International Journal of Multiphase Flow*, 72(2015) 188–197. <http://www.sciencedirect.com/science/article/pii/S0301932215000270>.
- [13] Endalew, A.K., Numerical modeling and experimental validation of heat pipes solar collector for water heating, *KTH Industrial Engineering, and Management*, Sweden, Master thesis ED1-2011-128MSC 2011.
- [14] Sandnes, J. Rekestad., A photovoltaic/thermal (PV/T) collector with a polymer absorber plate, experimental study, an analytical model, *Sol Energy* 2002;72: (2002) 63–73.
- [15] Zhao, X., Investigation of a novel heat pipe collector/CHP system., Nottingham University, England, Ph.D. (2003).
- [16] S. Sami., Prediction of Performance of a Novel Concept of Solar Photovoltaic- Thermal Panel and Heat Pipe Hybrid System, *International Journal of Modern Studies in Mechanical Engineering (IJMSME) Volume 5(1)(2019) 1-26*, ISSN 2454-9711 (Online), DOI: <http://dx.doi.org/10.20431/2454-9711>.
- [17] S.M. You, J.H. Kim, K.H. Kim, (2003), Effect of nanoparticles on critical heat flux of water in pool boiling heat transfer., *Appl. Phys. Lett.*, 83 (16) (2003), p. 3374 <http://scitation.aip.org/content/aip/journal/apl/83/16/10.1063/1.1619206>
- [18] K.H. Do, S.P. Jang, Effect of nanofluids on the thermal performance of a flat, micro heat pipe with a rectangular grooved wick, *Int. J. Heat Mass Transfer*, 53 (9–10) (2010), 2183-2192, 10.1016/j.ijheatmasstransfer.2009.12.020
- [19] Good, C., Chen, J., Dai, Y and Hestnes, A.G, Hybrid Photovoltaic-Thermal system: A Review. *Energie procedia*, 70(2015) 683-690.
- [20] G. Pei, Fu, H. Zhang and T. Jie., A numerical and experimental study on a heat pipe PV/T system, *Solar Energy* 85(5)(2011) 911-921.
- [21] M. Shafahi, V. Bianco, K. Vafai, O. Manca, An investigation of the thermal performance of cylindrical heat pipes using nanofluids., *Int. J. Heat Mass Transfer*, 53(2010) (1–3). 376-383, <http://linkinghub.elsevier.com/retrieve/pii/S0017931009005006>
- [22] Mohammad Alhuyi Nazari, Roghayeh Ghasempour, Mohammad H. Ahmadi., A review on using nanofluids in heat pipes, *Journal of Thermal Analysis and Calorimetry* 137(2019) 1847–1855.
- [23] M.Vijayakumara, P.Navaneethakrishnanb, G.Kumaresanc., Thermal characteristics studies on sintered wick heat pipe using CuO and Al₂O₃ nanofluids, *Experimental Thermal and Fluid Science*, 79(2016)(2017) 25-35
- [24] Tardy F., Sami S. M., Thermal analysis of heat pipes during thermal storage. *Applied Thermal Engineering*, 29(2009) 329–333
- [25] Coulson J. M., Richardson J. F., Marker J. H., Backhurst J. R., Coulson & Richardson's Chemical Engineering, Volume 1, Sixth edition Fluid Flow, Heat Transfer, and Mass Transfer, Butterworth – Heinemann Publishing, Oxford, UK., (1999).
- [26] P.K.Nagarajan, J.Subramani, S.Suyambazhahan, Ravishankar Sathyamurthy., Nanofluids for solar collector applications: A Review, The 6th International Conference on Applied Energy –

- ICAE2014, Energy Procedia 61 (2014) 2416 – 2434
- [27] http://www.engineeringtoolbox.com/fouling-heat-transfer-d_1661.html
- [28] Reay D.A., Kew P.A., Heat Pipes, 5th Edition, Butterworth-Heinemann publisher, Oxford, UK., (2006).
- [29] Tardy, F and Sami, S.M., An Experimental Study Determining Behaviour of Heat Pipes in Thermal Storage, International Journal of Ambient Energy, 29(3)(2008).
- [30] Sweidan, N. Ghaddara, and K. Chali, Optimized design and operation of a heat-pipe photovoltaic thermal system with phase change material for thermal storage, Journal of Renewable and Sustainable Energy 8, 023501 <https://doi.org/10.1063/1.4943091> (2016).
- [31] Sami, S. and Campoverde, C., Dynamic Simulation and Modeling of a Novel Combined Photovoltaic –Thermal Panel Hybrid System, International Journal of Sustainable Energy and Environmental Research, 7(1)(2018) 1-23.
- [32] Zhao Xuxin, Fu Huide, Ji Jie, Sun Hongyuan, Ma Rui, and Wu Qixing, Comparative study on performances of a heat-pipe PV/T system and a heat-pipe solar water heating system., International Journal of Green Energy, 13(3)(2016).
- [33] Sourav Diwania · Sanjay Agrawal · Anwar S. Siddiqui · Sonveer Singh, Photovoltaic–thermal (PV/T) technology: a comprehensive review on applications and its advancement, International Journal of Energy and Environmental Engineering (2020) 11:33–54 <https://doi.org/10.1007/s40095-019-00327-y>
- [34] Naghavi, M.S, Silaakhori, M, and Mehrali, M.S., Analytical thermal modeling of a heat pipe solar water heater system integrated with phase change material, Computer Applications in Environmental Sciences and Renewable Energy, ISBN: 978-960-474-370-4, (2015) 197-208.
- [35] Rajapakse, A, Chungpaibulpantana, S., Dynamic simulation of a photovoltaic refrigeration system., RERIC 16(3)(1994) 67-101.
- [36] <http://www.boulder.nist.gov/div838/theory/refprop/LINKING/Linking.htm#ExcelApplications>
- [37] Jens Glembin, Christoph Büttner, Jan Steinweg, and Gunter Rockendorf., Thermal Storage Tanks in High-Efficiency Heat Pump Systems – Optimized Installation and Operation Parameters, 9th International Renewable Energy Storage Conference, IRES 2015, Energy Procedia 73(2015) 331–340
- [38] Sami, S.M., ORC for low-Temperature Power Generation with low GWP Refrigerants., International Ambient Energy Journal, iFirst, (2012) 1-7.
- [39] Drilon Ferizaj, and Mohamad Kassem., Effect of nanofluids on the thermal performance of heat pipes, Bachelor of Science Thesis EGI-2014, KTH School of Industrial Engineering and Management Energy Technology EGI-2014 SE-100 44 STOCKHOLM, (2014).
- [40] Mohamed I Ali, Pawan K. Singh, Waka Tesfai, and Youssef Shatilla, An experimental study of heat pipe performance using nanofluids, International Conference on Applied Energy, ICAE (2012)5-8, Suzhou, China, Paper ID: ICAE2012- A10624
- [41] F. H. Fahmy, A. A. Nafeh, N. M. Ahamed and H. M. Farghally, A simulation model for Predicting the Performance of PV Powered Space Heating System in Egypt, RE&PQJ, 1(8)(2010) 1609-1616, <https://doi.org/10.24084/repqj08.734>.